ELSEVIER

Biophysical Chemistry 96 (2002) 173–190

Biophysical Chemistry

www.elsevier.com/locate/bpc

Thermodynamics of a diffusional protein folding reaction

Dieter Perl[a], Maik Jacob[a], Mikuláš Bánó[b], Marek Stupák[b], Marián Antalík[b,c], Franz X. Schmid[a,*]

[a]*Laboratorium für Biochemie and Bayreuther Zentrum für Molekulare Biowissenschaften, Universität Bayreuth, D-95440 Bayreuth, Germany*

[b]*Department of Biophysics, Institute of Experimental Physics, Slovak Academy of Sciences, SL-04353 Košice, Slovakia*

[c]*Department of Biochemistry, Faculty of Sciences, P.J. Šafárik University, SL-04254 Košice, Slovakia*

Received 19 March 2001; received in revised form 26 September 2001; accepted 1 October 2001

Abstract

The folding reactions of several proteins are well described as diffusional barrier crossing processes, which suggests that they should be analyzed by Kramers' rate theory rather than by transition state theory. For the cold shock protein *Bc*-Csp from *Bacillus caldolyticus*, we measured stability and folding kinetics, as well as solvent viscosity as a function of temperature and denaturant concentration. Our analysis indicates that diffusional folding reactions can be treated by transition state theory, provided that the temperature and denaturant dependence of the solvent viscosity is properly accounted for, either at the level of the measured rate constants or of the calculated activation parameters. After viscosity correction the activation barriers for folding become less enthalpic and more entropic. The transition from an enthalpic to an entropic folding barrier with increasing temperature is, however, apparent in the data before and after this correction. It is a consequence of the negative activation heat capacity of refolding, which is independent of solvent viscosity. *Bc*-Csp and its mesophilic homolog *Bs*-CspB from *Bacillus subtilis* differ strongly in stability but show identical enthalpic and entropic barriers to refolding. The increased stability of *Bc*-Csp originates from additional enthalpic interactions that are established after passage through the activated state. As a consequence, the activation enthalpy of unfolding is increased relative to *Bs*-CspB.

Keywords: Mechanism of protein folding; Cold shock protein; Folding kinetics; Viscosity; Denaturants

1. Introduction

Protein folding can be an extremely rapid process, and many small single-domain proteins reach their native states within a few milliseconds or even less. This is all the more remarkable, because these proteins typically fold in all-or-none $U \rightleftharpoons N$ two-state reactions without populating partially folded intermediates. The small two-state folders thus provide the unique opportunity to study folding reactions at an elementary level and, in particular, to characterize the properties of the activated states, which determine the rates of folding. Regions that are already native-like in the activated states of folding were identified by mutational

*Corresponding author. Tel.: +49-921-553660; fax: +49-921-553661.

E-mail address: fx.schmid@uni-bayreuth.de (F.X. Schmid).

0301-4622/02/$ - see front matter
PII: S0301-4622(02)00024-8

analyses [1–8]. The thermodynamic and physical properties of activated states such as enthalpy, entropy, solvent exposure and interactions with co-solvents, were characterized by varying temperature and solvent composition in the folding experiments [9–11].

The kinetics of protein folding have traditionally been analyzed by using transition state theory (TST), but the dependence on viscosity of several protein folding reactions [12–18] suggests that they are described more adequately as diffusional barrier crossing processes, as in Kramers' rate theory [11,19,20]. Both kinetic theories have strengths and weaknesses. TST allows the thermodynamic activation parameters $\Delta G^{\ddagger}$, $\Delta H^{\ddagger}$ and $\Delta S^{\ddagger}$ to be determined from the measured kinetics and their temperature dependence, but the absolute numbers calculated for $\Delta G^{\ddagger}$ and $\Delta S^{\ddagger}$ are unreliable, because the pre-exponential factor in the Eyring equation is not known for protein folding reactions [11]. Nevertheless, changes in the thermodynamic activation parameters, e.g. as a function of temperature or upon mutation, can be useful and interpretable. Kramers' theory provides a physically more appealing picture of the folding process because it describes a reaction as the diffusional motion across an energy barrier. In fact, Kramers' theory is being used by theoreticians to model the protein folding process [21,22].

The rate of a diffusional reaction and its temperature dependence are determined not only by the height of the energy barrier, but also by the decrease in solvent viscosity with temperature. Similarly, the dependence of the measured folding rates (λ) on denaturant concentrations (in the so-called Chevron plots) reports not only on the differential interactions of the native, unfolded and activated states of folding with the denaturant molecules, but is also influenced by the dependence of solvent viscosity on denaturant concentration.

We have been using the cold shock protein *Bs*-CspB from *Bacillus subtilis* to investigate elementary protein folding. *Bs*-CspB is a small single-domain protein of 67 residues with a five-stranded antiparallel β-sheet structure [23]. It folds and unfolds via a native-like activated state in a very fast viscosity-dependent $U \rightleftharpoons N$ two-state reaction without intermediates [15,16,24,25]. *Bc*-Csp (Fig. 1) from the thermophilic organism *Bacillus caldolyticus,* is a closely related, but thermostable homolog. It differs from *Bs*-CspB in amino acid sequence at 12 surface positions, but only two of them are responsible for the enhanced thermostability of *Bc*-Csp [26]. The backbone structures of the two proteins are virtually identical [27].

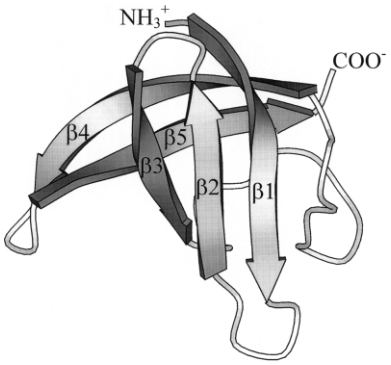

Fig. 1. Ribbon drawing of the tertiary structure of *Bc*-Csp. Five antiparallel β-strands (numbered) form a β-barrel. The N- and C-termini are marked. This MOLSCRIPT-figure [44] is based on the coordinates of Mueller et al. [27].

Although the two cold shock proteins differ two-fold in stability (at 25 °C), they refold at almost identical rates [28]. The additional stability of *Bc*-Csp relative to *Bs*-CspB originates predominantly from the 15-fold decrease in the rate of unfolding.

Here, we investigated equilibrium stability and folding kinetics of *Bc*-Csp as a function of both temperature and denaturant concentration, to determine how the stability curve of the thermophilic protein is changed and how the changes in equilibrium stability correlate with changes in the activation parameters.

Kramers' theory describes the folding kinetics of the cold shock proteins very well, and the rate constants for both unfolding and refolding decrease with solvent viscosity (η) [15,16]. At the same time, these folding reactions are also well described by the Eyring formalism and, in fact, before the viscosity dependence was known, the folding kinetics of *Bs*-CspB have been analyzed

by applying TST [24,25]. Solvent viscosity changes with both temperature and denaturant concentration. Therefore, we measured the folding kinetics as well as the solvent viscosities in a broad range of denaturant concentrations and temperatures. After correction of the kinetic data for the viscosity effect, the activation barriers of folding become less enthalpic and more entropic, but the general transition from an enthalpic barrier at low temperature to an entropic barrier at high temperature is still apparent in the data. The activated states for *Bs*-CspB and *Bc*-Csp are surprisingly similar in their thermodynamic properties.

2. Experimental

2.1. Materials

GdmCl and urea (ultrapure) were from ICN (Cleveland, OH, USA). All other chemicals were from Merck (Darmstadt, Germany). *Bc*-Csp and *Bs*-CspB were overexpressed in *E. coli* using the bacteriophage T7 RNA polymerase promoter system [29] and purified as described previously [24,27,28].

2.2. Heat-induced equilibrium unfolding transitions

Thermal unfolding transitions were measured in 0.1 M Na cacodylate/HCl, pH 7.0 at protein concentrations of 4 or 8 μM in the absence or presence of urea, GdmCl or NaCl at various concentrations. The transitions were monitored by the decrease of the CD signal at 222.6 nm at 1 or 0.5 cm path length in a JASCO J600 spectropolarimeter. Heating rates were 60 °C/h. Transitions were evaluated using a non-linear least squares fit according to a two-state model [30].

2.3. GdmCl-induced equilibrium unfolding transitions

Samples of *Bc*-Csp (1.5 μM) were incubated for 1 h in the presence of 0.1 M Na cacodylate/HCl, pH 7.0 and varying concentrations of GdmCl. The fluorescence of the samples was then measured at 343 nm (5 nm bandwidth) in a Hitachi F4010 fluorescence spectrometer at the desired temperature. The excitation wavelength was 280 nm (3 nm bandwidth). The experimental data were analyzed by assuming that the transition between the folded (N) and the unfolded (U) conformation is a two-state reaction, and that the fluorescence emissions of the native and the unfolded proteins depend linearly on GdmCl concentration. A non-linear least-squares fit [31] with proportional weighting of the experimental data was used to obtain the Gibbs free energy of stabilization as a function of the GdmCl concentration.

2.4. Stopped-flow kinetic experiments

A DX.17MV sequential mixing stopped-flow spectrometer from Applied Photophysics (Leatherhead, UK) was used for all kinetic measurements. The path length of the observation chamber was 2 mm and a 10 mM aqueous solution of cytidine-2′-phosphate in a 0.5-cm cell, was inserted between the observation chamber and the emission photomultiplier to absorb scattered light from the excitation beam. The folding kinetics were followed by the change in fluorescence above 300 nm after excitation at 280 nm (10 nm bandwidth).

All unfolding and refolding experiments were carried out in 0.1 M Na cacodylate/HCl pH 7.0. To initiate unfolding, typically 16.5 μM native *Bc*-Csp in buffer was diluted 11-fold with GdmCl solutions of varying concentrations to give final GdmCl concentrations between 1.0 and 6.5 M (depending on temperature). To initiate refolding, 16.5 μM unfolded *Bc*-Csp in concentrated GdmCl solutions (between 3 and 4.5 M, depending on temperature) was diluted 11-fold with aqueous buffer or with GdmCl solutions of varying concentrations to give final concentrations of 0.3–4 M GdmCl. Kinetics were measured at least eight times under identical conditions, averaged and analyzed as mono-exponential functions by using the software provided by Applied Photophysics.

2.5. Analysis of the folding kinetics

For a two-state folding reaction [Eq. (1)] the equilibrium constant K_{eq} is equal to the ratio of

the microscopic rate constants for unfolding (k_{NU}) and refolding (k_{UN}) [Eq. (2)], and the measured rate constant λ is equal to the sum of k_{NU} and k_{NU} [Eq. (3)]. Log k_{NU} and log k_{UN} are assumed to depend linearly on the denaturant concentration [Eqs. (4) and (5)]. In Eqs. (4) and (5), $m^{\ddagger}_{NU}$ and $m^{\ddagger}_{UN}$ are equal to $\partial\Delta G^{\ddagger}_{NU}/\partial$[GdmCl] and $\partial\Delta G^{\ddagger}_{NU}/\partial$[GdmCl], respectively.

$$\mathrm{N} \underset{k_{UN}}{\overset{k_{NU}}{\rightleftharpoons}} \mathrm{U} \tag{1}$$

$$K_{eq} = k_{NU}/k_{UN} \tag{2}$$

$$\lambda = k_{NU} + k_{UN} \tag{3}$$

$$-RT\ln k_{NU} = -RT\ln k_{NU}(H_2O) + m^{\ddagger}_{NU}[\mathrm{GdmCl}] \tag{4}$$

$$-RT\ln k_{UN} = -RT\ln k_{UN}(H_2O) + m^{\ddagger}_{UN}[\mathrm{GdmCl}] \tag{5}$$

$$k_{ij} = \left(\frac{k_B T}{h}\right)\left[\left(\frac{T}{T^0}\right)^{\left(\frac{\Delta C^{\ddagger}_{p,H_2O} + \Delta C^{\ddagger}_{p,i}[\mathrm{GdmCl}]}{R}\right)}\right] \times \exp\left[\frac{\Delta S^{\ddagger}_{H_2O}(T^0) + \Delta S^{\ddagger}_{i}(T^0)[\mathrm{GdmCl}]}{R} - \frac{\Delta H^{\ddagger}_{H_2O}(T^0) + \Delta H^{\ddagger}_{i}(T^0)[\mathrm{GdmCl}]}{RT} - \frac{(\Delta C^{\ddagger}_{p,H_2O} + \Delta C^{\ddagger}_{p,i}[\mathrm{GdmCl}])(T - T^0)}{RT}\right]. \tag{6}$$

In our analysis of the λ values we follow the procedure described by Schindler and Schmid [25]. Briefly, the entire set of λ values measured between 0.3 and 6.5 M GdmCl, and between 2 and 51 °C was subjected to a joint kinetic analysis based on the combination of Eqs. (2)–(6). In this analysis, which is based on TST, we decompose the activation Gibbs free energy $\Delta G^{\ddagger}$ into its (temperature-dependent) enthalpic and entropic components, $\Delta H^{\ddagger}$ and $\Delta S^{\ddagger}$. $\Delta H^{\ddagger}$ is assumed to depend linearly on temperature, i.e. the change in heat capacity going from the initial to the activated state, $\Delta C^{\ddagger}_{p}$, is assumed to be constant in the temperature range of our experiments (2–51 °C).

As the equilibrium thermodynamic parameters of unfolding, the activation parameters $\Delta G^{\ddagger}$, $\Delta H^{\ddagger}$, $\Delta C^{\ddagger}_{p}$ and $\Delta S^{\ddagger}$ are assumed to vary linearly with the denaturant concentration. The variation of $\Delta G^{\ddagger}$ with GdmCl concentration, $\Delta G^{\ddagger}_{i} = \partial\Delta G^{\ddagger}/\partial$[GdmCl], is identical with the kinetic *m* value, $\Delta H^{\ddagger}_{i} = \partial\Delta H^{\ddagger}/\partial$[GdmCl], $\Delta S^{\ddagger}_{i} = \partial\Delta S^{\ddagger}/\partial$[GdmCl], and $\Delta C^{\ddagger}_{p,i} = \partial\Delta C^{\ddagger}_{p}/\partial$[GdmCl].

2.6. Viscosity measurements

Viscosity was measured by the viscosity and density meter VISCODENS, developed in the Institute of Experimental Physics in Košice, Slovakia. It is a Couette-type non-contact viscometer, which measures the true bulk viscosity without errors originating from the contact of cylinders with the sample/air phase boundary. The inner cylinder of the instrument consists of a glass buoy with a diameter of 7.7 mm and a length of 63 mm, floating in the measured liquid. The outer cylinder with a diameter of 8.7 mm is also made of glass. In the upper part of the buoy is an SmCo magnet, and the buoy is equilibrated in the axis of the outer cylinder by the electromagnetic force. The vertical position is optically controlled. In the lower part of the buoy is a small aluminum cylinder located in the rotating magnetic field perpendicular to the axis. The interaction of this magnetic field with the eddy currents generated in the aluminum part causes rotation of the buoy. The angular velocity of this rotation is optically detected and used to calculate the viscosity. The measurement is controlled by a computer and performed at constant temperature or in scanning mode. The heating and cooling is provided by a thermoelectric element (Marlow Industries, Inc.), and the temperature is measured by a resistor thermometer with a precision of ~0.02 K.

The viscometer is calibrated by measuring the viscosity of water in the range of 20–85 °C and by comparison with tabulated reference data [32]. The precision of viscosity measurements is approximately 0.1%. The sample (approx. 1.5 ml) is kept at increased pressure (approx. 250 kPa) to avoid bubble formation at elevated temperature.

2.7. Correction of measured rate constants for solvent viscosity

The dependencies of the measured solvent viscosities η on temperature and denaturant concen-

tration ([D]) in Fig. 4 can be described by an empirical equation with nine parameters (a–i) [Eq. (7)].

$$\eta = \{a + b\exp[c[\mathrm{D}]]\} + \{d + e\exp[f[\mathrm{D}]]\}\exp\big[(g + h[\mathrm{D}] + i[\mathrm{D}]^2)(T - 273.15)\big]. \quad (7)$$

This equation has no physical meaning, but describes the dependence of viscosity on temperature and denaturant concentration very well. It was used to normalize the measured and the microscopic rate constants to a relative viscosity $\eta_{rel} = 1$ for water at 25 °C [see Eq. (11)].

2.8. Temperature dependence of viscosity

The viscosity of water decreases with temperature in an approximately exponential fashion. This suggests an alternative to the above described normalization of the reaction rates to a standard viscosity $\eta_{rel} = 1$ for water at 25 °C. The temperature dependence of η_{rel} at a given denaturant concentration can be approximated by an exponential term [Eq. (8)], which gives apparent contributions to the measured activation enthalpy $(\Delta H^{\ddagger})_{corr}$ and activation entropy $(\Delta S^{\ddagger})_{corr}$ [Eqs. (8) and (9)]. This empirical treatment has no physical implications. In particular, it does not imply that diffusion involves transitions over energy barriers.

$$\eta_{rel} = \exp\left(-\frac{(\Delta G^{\ddagger})_{corr}}{RT}\right) = \exp\left(\frac{(\Delta S^{\ddagger})_{corr}}{R}\right)\exp\left(-\frac{(\Delta H^{\ddagger})_{corr}}{RT}\right) \quad (8)$$

$$\frac{\partial \ln \eta_{rel}}{\partial 1/T} = -\frac{(\Delta H^{\ddagger})_{corr}}{R}. \quad (9)$$

3. Results and discussion

3.1. Equilibrium stability

Bc-Csp is approximately twice as stable as its mesophilic homolog *Bs*-CspB at pH 7 and 25 °C. Under these conditions the midpoint of the urea-induced unfolding transition of *Bc*-Csp is above 7 M, and 10 M urea cannot unfold *Bc*-Csp completely. Therefore, we used the strong, but ionic denaturant GdmCl in all experiments. GdmCl-induced equilibrium unfolding transitions (Fig. 2a) were measured at 13 temperatures between 2 and 48 °C, and thermal unfolding transitions (Fig. 2b) were measured at 20 different GdmCl concentrations ranging from 0 to 1.4 M.

Bc-Csp is, among others, stabilized by electrostatic interactions at the protein surface. Therefore, its thermal stability decreases slightly when these favorable interactions are screened by adding 0–0.5 M NaCl [27]. At higher salt concentrations the stability increases linearly, probably as a consequence of general Hofmeister effects (Fig. 2c). The non-linearity caused by electrostatic screening is also evident in the data obtained from the thermal unfolding transitions in the presence of GdmCl (Fig. 2c). The linear extrapolations of the stabilities as obtained at high NaCl or GdmCl concentrations thus underestimate stability in the absence of salt in both cases by approximately 3 kJ/mol (Fig. 2c), because they do not account for the favorable ionic interactions in *Bc*-Csp that are screened in ≥ 0.5 M salt. Urea is an uncharged denaturant and thus does not screen electrostatic interactions. The ΔG_D values from thermal unfolding depend linearly on urea concentration between 0 and 2 M urea (Fig. 2c).

Thermal unfolding transitions at different denaturant concentrations and denaturant-induced transitions at different temperatures can be combined to determine the stability curve of a protein, i.e. the dependence on temperature of the Gibbs free energy of denaturation, ΔG_D, over a wide temperature range [33]. Fig. 3a gives the stability curve of *Bc*-Csp as determined at 1.2 M GdmCl. At this GdmCl concentration, the stability depends linearly on salt concentration and long extrapolations of the thermal transitions in the presence of GdmCl can be avoided. The curvature in the stability data gives a value of 3.8 kJ/(mol·K) for ΔC_p and shows that the stability is highest at approximately 11 °C. The data from the thermal transition at 1.2 M GdmCl and from the GdmCl-induced transitions at various temperatures, coincide very well because all measurements were performed at high salt.

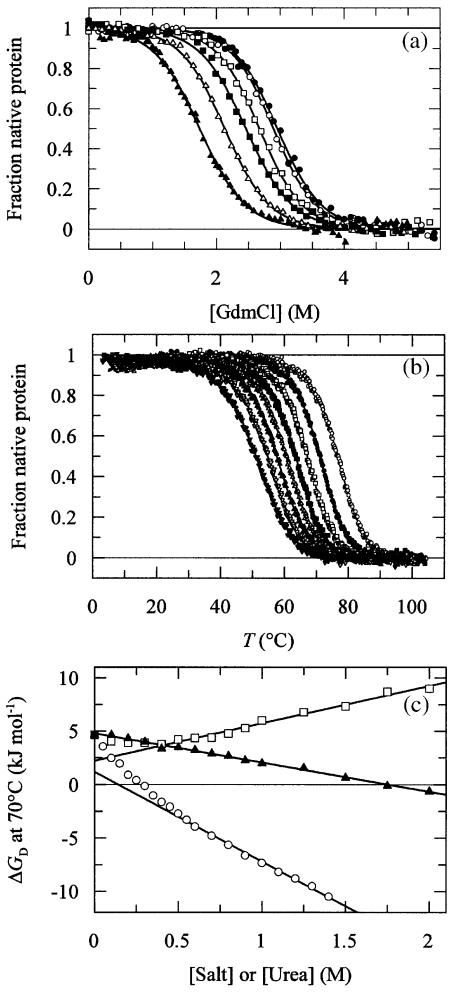

Fig. 2. (a) GdmCl-induced equilibrium unfolding transitions of *Bc*-Csp at 2 (○), 13 (●), 25 (□), 35 (■), 40 (△) and 48 °C (▲). (b) Thermal unfolding transitions of *Bc*-Csp in the presence of 0 (○), 0.2 (●), 0.4 (□), 0.6 (■), 0.8 (△), 1 (▲), 1.2 (▽) and 1.4 M (▼) GdmCl. (c) Free energy of unfolding ΔG_D of *Bc*-Csp at 70 °C as a function of the NaCl (□), GdmCl (○) and urea (▲) concentrations. For evaluation, the heat capacity ΔC_p was fixed to 3.3 kJ/(mol·K). All measurements were performed in 0.1 M Na cacodylate/HCl, pH 7.0 as described in Sections 2.2 and 2.3. In panel (a) and (b), the fractions of native protein as obtained after two-state $N \rightleftharpoons U$ analyses of the data [30,31] are shown as a function of the GdmCl concentration and temperature, respectively. The continuous lines represent the results of least-squares fit analyses based on the two-state unfolding mechanism. In panel (c), the continuous lines result from linear fits of the data points above 0.5 M salt for NaCl and GdmCl data, and of all data points for urea.

This is not the case for the dependence of ΔG_D on temperature in 0 M GdmCl (Fig. 3b). The ΔG_D values derived from the thermal unfolding transition reflect the stability at low salt concentration where the favorable ionic interactions in *Bc*-Csp are not screened. The ΔG_D values

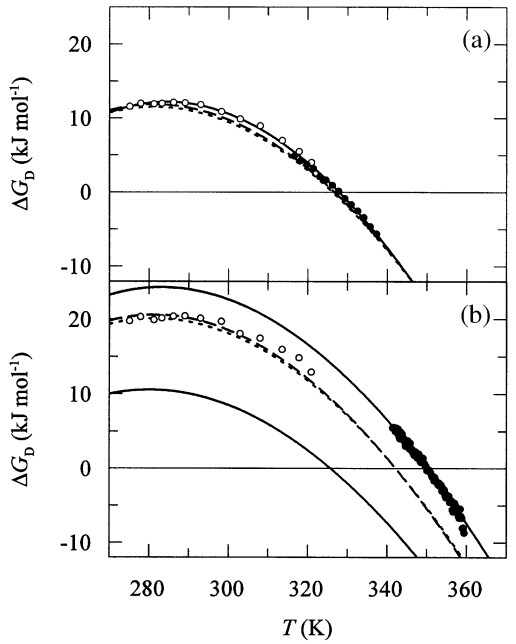

Fig. 3. Stability curves for *Bc*-Csp in (a) 1.2 and (b) 0 M GdmCl, 0.1 M Na-cacodylate pH 7.0. (a) ΔG_D was derived from GdmCl-induced unfolding transitions at 13 different temperatures (○), and from a thermal unfolding transition (●). The joint fit of these data based on a two-state model is shown by the continuous curve ($\Delta C_p = 3.8 \pm 0.1$ [kJ/(mol·K)], ΔH(25 °C) = 64.6 ± 1.2 (kJ/mol), ΔS(25 °C) = 180 ± 4 [J/(mol·K)]). The results for 1.2 M GdmCl from the joint fit of the kinetic data of Fig. 5 without viscosity correction (dotted curve) ($\Delta C_p = 3.4 \pm 0.1$ [kJ/(mol·K)], ΔH (25 °C) = 68.0 ± 0.9 (kJ/mol), ΔS (25 °C) = 195 ± 4 [J/(mol·K)]), and after viscosity correction (broken curve) ($\Delta C_p = 3.4 \pm 0.1$ [kJ/(mol·K)], ΔH (25 °C) = 68.9 ± 0.9 (kJ/mol), ΔS (25 °C) = 197 ± 4 [J/(mol·K)]) are also shown. (b) ΔG_D at 0 M GdmCl (upper continuous curve) derived from a thermal unfolding transition (●) with a fixed ΔC_p of 3.3 kJ/(mol·K). The data, as extrapolated linearly from the GdmCl-induced transitions to 0 M GdmCl (b), were not included in the fit. The results for 0 M GdmCl from the joint fit of the kinetic data of Fig. 5, before and after the viscosity correction are shown by the dotted and broken curves, respectively. The corresponding stability curve for *Bs*-CspB (lower continuous curve) is taken from Schindler and Schmid [25].

extrapolated linearly from the GdmCl-induced transitions at various temperatures reflect the stability at high salt and thus underestimate the stability by approximately 3 kJ/mol (see Fig. 2c). As a consequence, these extrapolated values fall to approximately 3 kJ/mol below the stability curve extrapolated from the thermal unfolding transition. The latter curve was calculated by using a ΔC_p value of 3.3 kJ/(mol·K), as obtained from the analysis of the folding kinetics (see below).

Fig. 3b also shows the stability curve for the mesophilic homolog *Bs*-CspB, calculated from the data given in Table 2 of Schindler and Schmid [25]. The curve for *Bc*-Csp is shifted upwards relative to this reference, but the temperature of maximum stability and the curvature are essentially unchanged. *Bc*-Csp is thus more stable than *Bs*-CspB at all temperatures.

3.2. Viscosities of GdmCl and urea solutions

The viscosities of 0–6.6 M GdmCl solutions in 0.1 M Na cacodylate, pH 7.0 (the buffer used in our experiments for *Bc*-Csp) were measured as a function of temperature between 10 and 50 °C (Fig. 4a). In the previous kinetic experiments with *Bs*-CspB urea was used as a denaturant [25] and therefore viscosities of 0–9.5 M urea solutions in the same buffer were also measured (Fig. 4c). The viscosity of pure water (broken line) was taken from Weast [32]. GdmCl and urea increase the solvent viscosity in a non-linear fashion with a particularly strong increase at high denaturant concentrations, as observed previously by Kawahara and Tanford at 25 °C [34]. At all concentrations, the solvent viscosity decreases with temperature in an approximately exponential manner. This becomes evident when the viscosities are shown in the form of pseudo Arrhenius plots (Fig. 4b,d). This representation reveals that between 0 and 4 M the relative decrease with temperature of solvent viscosity becomes slightly smaller and that all curves are slightly bent upwards with decreasing temperature. Above 3 M the viscosity of GdmCl solutions increases more strongly with denaturant concentration than in the case of urea (Fig. 4e).

The measured temperature dependence of the rate of a diffusional reaction reflects (i) the height of the energy barrier of the reaction itself, and (ii) the decrease in solvent viscosity with temperature. To determine the contribution of solvent viscosity it is helpful to analyze its dependence on temperature as if it were a chemical reaction [see Eqs. (8) and (9)]. Such treatments (as in Fig. 4b,d) have no physical meaning, but they provide pseudo activation parameters, $(\Delta X^{\ddagger})_{corr}$, which can be used to correct the activation parameters that were calculated, e.g. based on TST, $(\Delta X^{\ddagger})_{calc}$, for the contributions that originate from the temperature-dependent decrease in solvent viscosity [Eq. (8)]

$$\Delta X^{\ddagger} = (\Delta X^{\ddagger})_{calc} + (\Delta X^{\ddagger})_{corr}. \quad (10)$$

These pseudo activation parameters are shown in Table 1 for 0–6.6 M GdmCl and for 0–9.5 M urea. Both sets of data are based on a relative viscosity of 1 for the water viscosity at 25 °C. $(\Delta G^{\ddagger})_{corr}$ is generally very small, because additions of 6.6 M GdmCl or 9.5 M urea increase the solvent viscosity by less than a factor of two. $(\Delta H^{\ddagger})_{corr}$ and $(\Delta S^{\ddagger})_{corr}$ are, however, large because the relative solvent viscosity depends strongly on temperature (Fig. 4b,d). $(\Delta H^{\ddagger})_{corr}$ is −17.1 kJ/mol in buffer at 25 °C and −13.7 kJ/mol in the presence of 6.6 M GdmCl. Since $(\Delta G^{\ddagger})_{corr}$ is very small, the $(\Delta H^{\ddagger})_{corr}$ values are opposed by almost equal $T(\Delta S^{\ddagger})_{corr}$ values. The small curvatures in the pseudo Eyring plots in Fig. 4b,d lead to a slight decrease of $(\Delta H^{\ddagger})_{corr}$ with temperature, equivalent to a very small value for $(\Delta C_p^{\ddagger})_{corr}$ of approximately 0.1 kJ/(mol·K).

The apparent activation enthalpies, $(\Delta H^{\ddagger})_{calc}$, as calculated from Eyring plots are thus larger than the 'true' activation enthalpies, $\Delta H^{\ddagger}$. There is no need to correct the measured activation heat capacities of unfolding and refolding because the values of approximately 0.1 kJ/(mol·K) for $(\Delta C_p^{\ddagger})_{corr}$ (Table 1) are smaller than the confidence limits of experimental activation heat capacities.

The data in Table 1 reflect how, for a diffusional reaction, the calculated activation enthalpies differ from the true activation enthalpy and how the $(\Delta H^{\ddagger})_{corr}$ values can be used to correct the experimental values. We used, however, an alternative approach and corrected the measured rate constants (as a function of temperature and denaturant con-

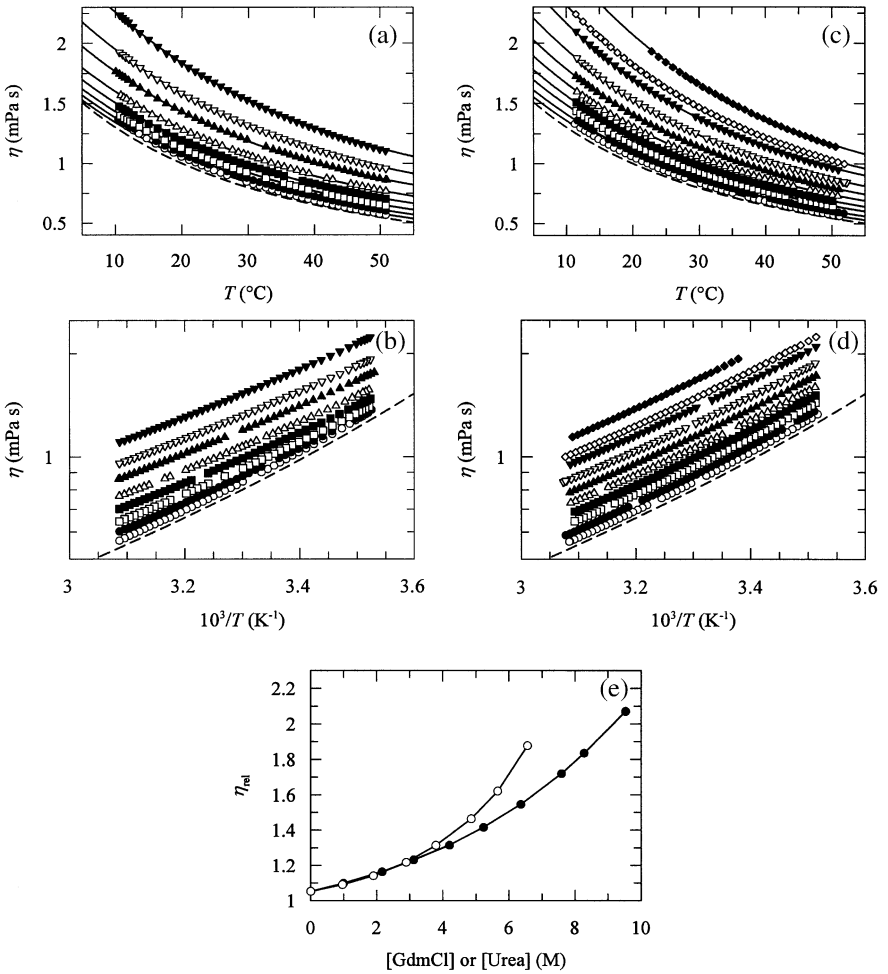

Fig. 4. Viscosity of aqueous GdmCl and urea solutions. (a) Viscosities of 0 (○), 1.0 (●), 1.9 (□), 2.9 (■), 3.8 (△), 4.9 (▲), 5.7 (▽) and 6.6 M (▼) GdmCl in 0.1 M Na cacodylate, pH 7.0. (b) Replot of the data of panel (a) in the form of an Arrhenius diagram. (c) Viscosities of 0 (○), 1.0 (●), 2.2 (□), 3.1 (■), 4.2 (△), 5.2 (▲), 6.4 (▽), 7.6 (▼), 8.3 (◇) and 9.5 M (◆) urea in 0.1 M Na cacodylate. (d) Replot of the data of panel (c) in the form of an Arrhenius diagram. The broken curves represents the viscosity of water calculated according to Weast [32]. The curves represent the fit based on Eq. (7) with the following parameters. GdmCl: $a=0.1780$, $b=0.1225$, $c=0.2028$, $d=1.4376$, $e=0.01674$, $f=0.5802$, $g=-0.0331$, $h=0.0004424$, and $i=2.272\times10^{-8}$; urea: $a=0.1341$, $b=0.1670$, $c=0.1155$, $d=1.3206$, $e=0.1657$, $f=0.2302$, $g=-0.0339$, $h=0.0003582$, and $i=-3.244\times10^{-5}$. E: viscosities of GdmCl (○) and urea (●) solutions in 0.1 M Na cacodylate, pH 7.0 at 25 °C relative to the viscosity of water at 25 °C.

centration) for the viscosity effect. In this approach the entire set of η values in Fig. 4a was fitted to an empirical equation with nine parameters [Eq. (7)], and these values were then used to calculate rate constants (k_0), that are normalized to the viscosity of water at 25 °C ($\eta_0=0.8904$ mPa·s) from the rate constants (k), measured at different temperatures and denaturant concentrations [Eq. (11)].

$$k_0=k\frac{\eta}{\eta_0}=k\eta_{\mathrm{rel}}. \tag{11}$$

Table 1
Eyring analysis of the viscosities of solutions at 25 °C[a]

(*a*) *GdmCl*										
[GdmCl] (M)	0	1.0	1.9	2.9	3.8	4.9	5.7	6.6		
$(\Delta G^{\ddagger})_{corr}$ (kJ/mol)	−0.1	−0.2	−0.3	−0.5	−0.7	−0.9	−1.2	−1.6		
$(\Delta H^{\ddagger})_{corr}$ (kJ/mol)	−17.1±0.1	−16.0±0.1	−15.2±0.1	−14.5±0.1	−14.0±0.1	−13.7±0.1	−13.6±0.1	−13.7±0.1		
$(\Delta S^{\ddagger})_{corr}$ [J/(mol·K)]	−56.9±0.1	−53.1±0.1	−49.9±0.1	−47.0±0.1	−44.8±0.1	−42.8±0.1	−41.6±0.1	−40.8±0.1		
$(\Delta C_p^{\ddagger})_{corr}$ [J/(mol·K)]	118±3	98±2	89±3	76±2	45±1	69±3	71±3	71±2		
(*b*) *Urea*										
[GdmCl] (M)	0.0	1.0	2.2	3.1	4.2	5.2	6.4	7.6	8.3	9.5
$(\Delta G^{\ddagger})_{corr}$ (kJ/mol)	−0.1	−0.2	−0.4	−0.5	−0.7	−0.9	−1.1	−1.3	−1.5	−1.8
$(\Delta H^{\ddagger})_{corr}$ (kJ/mol)	−17.1±0.1	−16.7±0.1	−16.3±0.1	−16.1±0.1	−15.8±0.1	−15.7±0.1	−15.6±0.1	−15.8±0.1	−15.8±0.1	−16.0±0.1
$(\Delta S^{\ddagger})_{corr}$ [J/(mol·K)]	−56.9±0.1	−55.2±0.1	−53.5±0.1	−52.1±0.1	−50.6±0.1	−49.7±0.1	−48.9±0.1	−48.4±0.1	−48.0±0.1	−47.5±0.1
$(\Delta C_p^{\ddagger})_{corr}$ [J/(mol·K)]	111±2	104±2	103±2	97±2	95±2	88±2	92±2	92±2	91±2	80±3

[a] Viscosities of solutions of GdmCl and urea in 0.1 M Na cacodylate, pH 7.0 were related to the viscosity of water at 25 °C of 0.8904 cP. $(\Delta G^{\ddagger})_{corr}$, activation Gibbs free energy, $(\Delta H^{\ddagger})_{corr}$, activation enthalpy, $(\Delta S^{\ddagger})_{corr}$, activation entropy, $(\Delta C_p^{\ddagger})_{corr}$, activation heat capacity derived from the fit of the data to Eqs. (8) and (9).

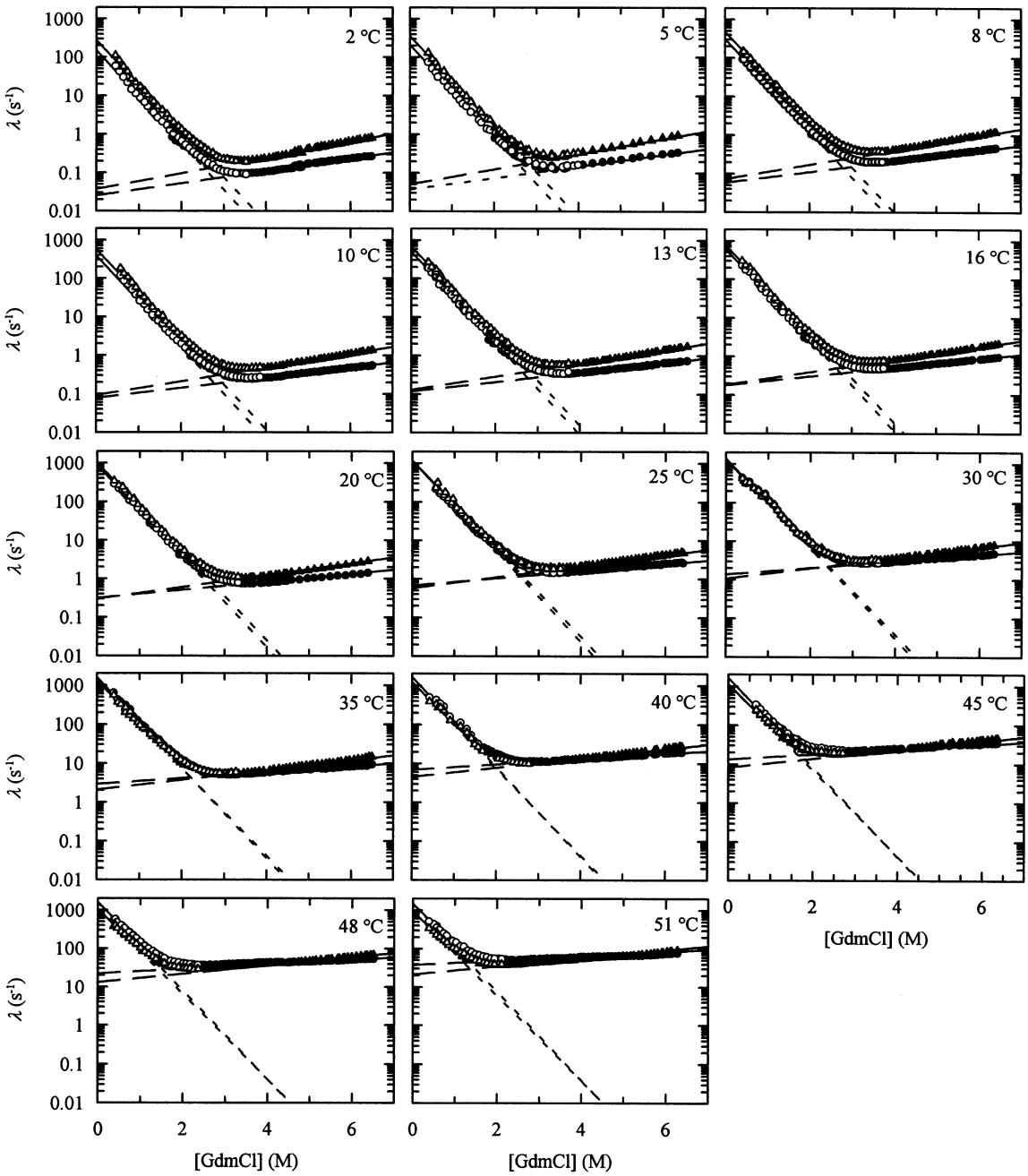

Fig. 5. Dependence on GdmCl concentration of the rate constant λ of refolding (open symbols) and unfolding (closed symbols) of *Bc*-Csp at 14 temperatures before (○, ●) and after the viscosity correction (△, ▲). All 1309 data points were subjected to a joint fit to Eqs. (2)–(6). The parameters for these fits are given in Table 2a. The profiles for the apparent rate constant λ (continuous lines), the rate constants of unfolding, k_{NU} (broken lines) and refolding, k_{UN} (dotted lines) as calculated from this fit are shown.

Table 2
Activation parameters of folding reactions at 25 °C[a]

Parameter[b]	Uncorrected data			With viscosity correction for GdmCl		
	U→‡	N→‡	N⇌U	U→‡	N→‡	N⇌U
(*a*) *Bc-Csp*						
ΔH (H_2O) (kJ/mol)	32.6±0.5	107.4±0.6	74.9±0.8	16.3±0.5	93.0±0.6	76.7±0.8
ΔH_i [kJ/(mol·M)])	2.1±0.4	−3.6±0.1	−5.7±0.4	3.0±0.4	−3.5±0.1	−6.5±0.4
ΔS (H_2O) [J/(mol·K)]	−77±2	112±2	189±3	−131±2	62±2	194±3
ΔS_i [J/(mol·K·M)]	−16±2	−10±1	5±2	−12±2	−9±1	3±2
ΔC_p (H_2O) [kJ/(mol·K)]	−2.2±0.1	1.1±0.1	3.3±0.1	−2.1±0.1	1.2±0.1	3.3±0.1
$\Delta C_{p,i}$ [J/(mol·K·M)]	−2±50	82±17	84±53	12±50	63±18	51±53
ΔG (H_2O) (kJ/mol)	55.5	74.0	18.5	55.5	74.4	18.8
M [kJ/(mol·M)]	6.7	−0.5	−7.2	6.5	−0.8	−7.3
(*b*) *Bs-CspB*[c]						
ΔH (H_2O) (kJ/mol)	31.6±2.2	96.1±3.3	64.4±4.0	15.4±2.1	81.0±3.3	65.6±4.0
ΔH_i [kJ/(mol·M)])	−2.4±1.6	−1.3±0.5	1.1±1.6	−2.0±1.5	−1.4±0.5	0.6±1.6
ΔS (H_2O) [J/(mol·K)]	−81±7	106±11	186±13	−135±7	55±11	189±13
ΔS_i [J/(mol·K·M)]	−17±5	−4±2	13±6	−15±5	−4±2	12±6
ΔC_p (H_2O) [kJ/(mol·K)]	−2.7±0.3	0.3±0.4	3.0±0.5	−2.6±0.3	0.5±0.4	3.1±0.5
$\Delta C_{p,i}$ [J/(mol·K·M)]	−66±135	149±70	216±152	−80±133	128±70	208±150
ΔG (H_2O) (kJ/mol)	55.7	64.6	8.9	55.6	64.8	9.2
M [kJ/(mol·M)]	2.7	−0.1	−2.8	2.5	−0.3	−2.8

[a] The activation parameters for refolding (U→‡) and unfolding (N→‡) are the result of a joint fit of all 1309 rate constants measured between 0.3 and 6.5 M GdmCl, and 2 and 51 °C according to Eqs. (1)–(6), either with or without correction of the measured rates for solvent viscosity according to Eq. (11). Equilibrium parameters for unfolding (N⇌U) are the difference between activation parameters of unfolding and refolding. Measurements were performed in 0.1 M Na cacodylate, pH 7.0. N, U and ‡ denote the native, unfolded, and transition states, respectively.

[b] ΔX (H_2O), thermodynamic parameter in the absence of GdmCl or urea at 25 °C, ΔX_i, GdmCl or urea dependence of the thermodynamic parameter at 25 °C, with X being either the reaction enthalpy H, the reaction entropy S, or the heat capacity C_p. ΔG_D (H_2O), Gibbs free energy in the absence of GdmCl or urea at 25 °C. m, dependence of ΔG_D on GdmCl or urea at 25 °C. No errors for ΔG_D (H_2O) and m are given because these parameters do not result from the fit.

[c] Taken from Schindler and Schmid [25].

3.3. Unfolding and refolding kinetics of Bc-Csp as a function of GdmCl concentration and temperature

The kinetics of unfolding and refolding were measured by the change in protein fluorescence after stopped-flow dilutions of the native and unfolded protein, respectively, to the final conditions. Folding was reversible under all conditions (0–7 M GdmCl, 2–51 °C), and the kinetics followed single exponential time courses.

The measured rate constants λ of unfolding and refolding of *Bc*-Csp are shown in Fig. 5 as a function of the GdmCl concentration at 14 temperatures between 2 and 51 °C. The values for logλ follow a V-shaped dependence on denaturant concentration, which is commonly referred to as an (inverted) chevron. As in the previous experiments at 25 °C, no evidence for folding intermediates could be found. The observed amplitudes accounted for the entire change in fluorescence at all temperatures and GdmCl concentrations, and there is no evidence for a roll-over in the refolding

or unfolding kinetics in Fig. 5. At all temperatures the chevrons are strongly asymmetric with high $m^{\ddagger}$ values for refolding and low $m^{\ddagger}$ values for unfolding, which suggests that the activated state of folding resembles the native state in its interactions with the denaturant molecules in the solvent.

Fig. 5 shows the values for λ both before and after the correction for solvent viscosity. As outlined above, the data were normalized relative to the viscosity of water at 25 °C, therefore the differences are smallest for the refolding data at 25 °C. The influence of the denaturant on solvent viscosity is small between 0 and 2 M GdmCl (Fig. 4), and therefore the slopes of the refolding limbs of the chevrons (the $m^{\ddagger}$ values) in Fig. 5 are virtually unaffected by the viscosity correction. This is borne out by the quantitative analysis of the data in Fig. 5 (see below). At high GdmCl concentration the solvent viscosity increases markedly (Fig. 4), and therefore the corrected rates of unfolding increase progressively relative to the uncorrected values, leading to a marked increase in the $m^{\ddagger}$ value for unfolding. The temperature dependencies of both unfolding and refolding rates are decreased by the viscosity correction and therefore the corrected rate constants are higher than the measured values below 25 °C, but smaller above 25 °C.

3.4. Influence of solvent viscosity on the activation parameters

This visual inspection of the original and the viscosity-corrected kinetic data in Fig. 5 thus indicates that the correction has two consequences. The activation enthalpies for both unfolding and refolding become smaller, and the $m^{\ddagger}$ value for unfolding increases. To assess these consequences quantitatively, we analyzed the folding kinetics before and after the viscosity correction by using transition state theory (TST). Analyses based on Kramers' theory and TST are not mutually exclusive [20]. We use TST here to demonstrate how the correction for viscosity affects the calculated activation parameters of a diffusional folding reaction, but we are aware that the absolute numbers for $\Delta G^{\ddagger}$ and $\Delta S^{\ddagger}$ are unreliable, because the pre-exponential factors in both the Eyring and Kramers equations are not known for protein folding reactions. Nevertheless, changes in these activation parameters, e.g. as a function of the conditions, can be interpreted. The values for $\Delta H^{\ddagger}$ and $\Delta C_p^{\ddagger}$ are reliable, because they are derived directly from the temperature dependence of the rate constants for unfolding and refolding.

The entire set of 1309 λ values between 2 and 51 °C, and between 0.3 and 6.5 M GdmCl measured for *Bc*-Csp (Fig. 5), was subjected to a joint analysis based on Eqs. (2)–(6). In this analysis, the activation parameters $\Delta H^{\ddagger}$, $\Delta S^{\ddagger}$ and $\Delta C_p^{\ddagger}$ were assumed to vary linearly with the GdmCl concentration, and the values for $\Delta C_p^{\ddagger}$ were assumed to be independent of temperature. All kinetic data were obtained above 0.3 M GdmCl, and under these conditions we found no deviation from linearity in the slopes of the chevrons in Fig. 5, suggesting that the $\Delta G^{\ddagger}$ values for unfolding and refolding depend linearly on the denaturant concentration in this range of conditions.

The resulting kinetic parameters calculated for 25 °C are shown in Table 2, a graphical representation of the changes in H, $-T\,S$ and ΔC_p during folding at three temperatures is provided by Fig. 6. The correction to the viscosity of water at 25 °C lowers the $\Delta H^{\ddagger}$ values for unfolding by 14.4 kJ/mol and for refolding by 16.3 kJ/mol, which implies that the actual enthalpy barriers are significantly lower than the measured values. As outlined above, this originates from the decrease of solvent viscosity with temperature.

The free energies of activation, $\Delta G^{\ddagger}$, for unfolding and refolding are virtually unaffected by the viscosity correction because at 25 °C, the addition of 6 M GdmCl increases the relative viscosity of the solvent less than two-fold. As a consequence, the decreases in the $\Delta H^{\ddagger}$ values are accompanied by concomitant decreases in the $T\Delta S^{\ddagger}$ values of 16.1 and 14.9 kJ/mol for refolding and unfolding, respectively. Consequently, ignoring the temperature dependence of the solvent viscosity leads to an overestimation of the enthalpic barrier and an underestimation of the entropic barrier of refolding (Fig. 6b,c).

The activation heat capacities $\Delta C_p^{\ddagger}$ of unfolding and refolding are virtually unaffected by the viscosity correction. Both increase by 0.1 kJ/(mol·K) (Table 2) as expected from the dependence on

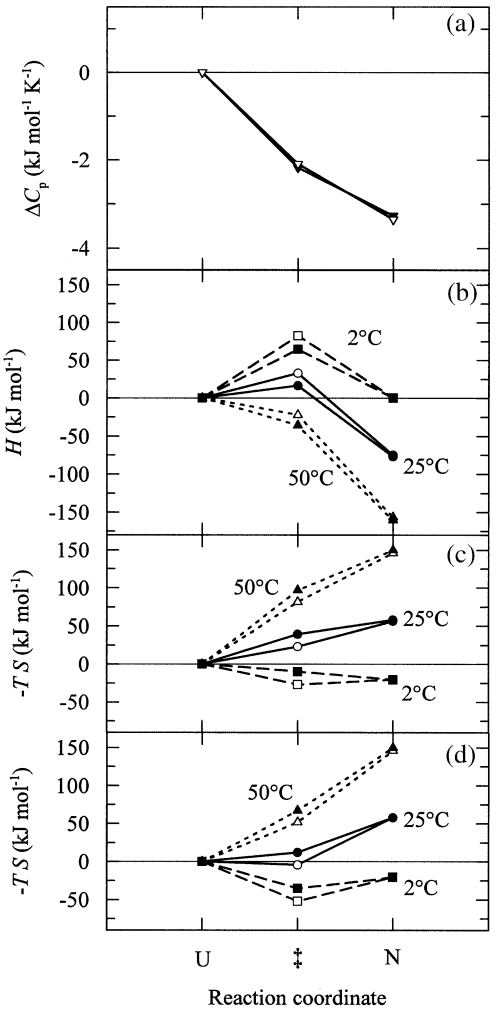

Fig. 6. Reaction profiles for the folding reaction of *Bc*-Csp in 0 M GdmCl, pH 7.0 when going from the unfolded state (U) via the transition state (‡) to the folded state (N). The open and closed symbols refer to the analyses before and after the viscosity correction, respectively. The parameters for ‡ and N were calculated from the difference relative to the values for the unfolded state U that were set to zero. The heat capacity [panel (a)] was assumed to the independent of temperature. The enthalpy H [panel (b)] and the entropic term $-TS$ [panel (c) and (d)] are shown for 2 (squares, broken lines), 25 (circles, continuous lines) and 50 °C (triangles, dotted lines). $-TS$ values calculated with pre-exponential factors in the Eyring equation of 6×10^{12} and 10^{8} s^{-1} at 25 °C are shown in panels (c) and (d), respectively.

temperature of the solvent viscosities (Fig. 4b). The $m^{\ddagger}$ value for refolding is only marginally changed [from 6.7 to 6.5 kJ/(mol·M)] by the viscosity correction, because the refolding kinetics are measured at low GdmCl concentration. The $m^{\ddagger}$ value for unfolding changes from -0.5 to -0.8 kJ/(mol·M), because the kinetic data that determine the GdmCl dependence of the unfolding rate are measured at high denaturant concentration, where the viscosity increases significantly. This leads to the small tilts in the chevron plots in Fig. 5, and thus the folding transition state appears a bit less native-like after the viscosity correction, as judged by the $m^{\ddagger}$-value criterion.

The activation parameters in Table 2 were used to calculate the microscopic rate constants of unfolding and refolding, k_{NU} and k_{UN}, as a function of temperature. The resulting values for $\lambda = k_{NU} + k_{UN}$ are shown in Fig. 5 as continuous lines. They follow the experimental data very well in the entire range of temperatures and GdmCl concentrations. Fig. 7 shows k_{NU} and k_{UN} as a function of temperature at 0, 3.5 and 7 M GdmCl.

The viscosity correction affects only the kinetics, but not the equilibrium stability of *Bc*-Csp. The equilibrium thermodynamic parameters, as obtained from the differences of the activation parameters for unfolding and refolding, are identical before and after the correction (Table 2). Moreover, the data obtained for 1.2 M GdmCl coincide within experimental uncertainty with the equilibrium parameters as obtained from the analysis of the thermal and denaturant-induced unfold-

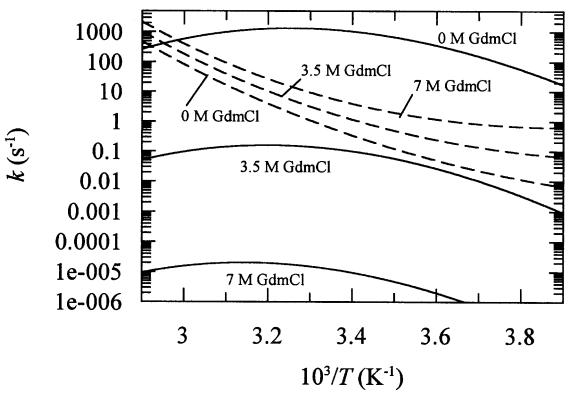

Fig. 7. Arrhenius plots of the microscopic rate constants of unfolding k_{NU} (broken lines) and refolding k_{UN} (solid lines) of *Bc*-Csp in 0, 3.5 and 7 M GdmCl. The lines were calculated from the parameters after viscosity correction given in Table 2a.

ing transitions (Fig. 3a,b). A slight difference in the ΔC_p values [3.4 kJ/(mol·K)] as derived from the kinetics and 3.8 kJ/(mol·K) as derived from the equilibrium data) leads to a small difference in the curvature of the two stability profiles in Fig. 3. A similar deviation was observed for *Bs*-CspB before [25] and reflects the large uncertainty in the ΔC_p values, which are obtained from the second derivative of the measured rate and equilibrium constants. The ΔG_D values that were calculated from the kinetic data and extrapolated to 0 M GdmCl (Fig. 3b), coincide with the ΔG_D values as derived from the GdmCl-induced equilibrium transitions. In both cases, the experimental data obtained at high salt concentrations are extrapolated linearly to 0 M GdmCl and therefore lack the electrostatic contribution of approximately 3 kJ/mol to stability.

Sixty-four percent of the overall change in heat capacity occurs between the unfolded and the activated state of folding (Fig. 6a), suggesting that by the ΔC_p criterion the activated state of folding of *Bc*-Csp is only approximately two thirds native-like. For *Bs*-CspB, the activated state was approximately 90% native. We are not sure whether this difference in the 'native character' of the activated state is significant. The values for $\Delta C_p^{\ddagger}$ are derived from the second derivative of the measured rate constants and thus reflect the curvature in a conventional Arrhenius diagram. It is often, but not always, observed that the analyses of the $m^{\ddagger}$ and the $\Delta C_p^{\ddagger}$ values give similar values for the 'native-like' character of a folding transition state [35,36]. It should be noted that the *m* values report on the interaction of the protein with denaturant molecules, whereas ΔC_p reports on changes in the hydration of hydrophobic and polar groups [37,38].

Panels (b) and (c) of Fig. 6 show the enthalpic (H) and the entropic ($T\,S$) contributions to the activation barrier of folding of *Bc*-Csp at three temperatures. The values for the unfolded protein are arbitrarily set to zero in these comparisons. These profiles visualize that the neglect of the viscosity correction generally leads to an overestimation of the enthalpic and an underestimation of the entropic barrier of folding. The corrections are relatively large for refolding at 25 °C, where the enthalpic barrier is twofold decreased and the entropic barrier two-fold increased after accounting for solvent viscosity. However, before as well as after correction, the profiles in Fig. 6b,c indicate that in the range of physiological temperatures, there is a pronounced transition from an enthalpic barrier (at low temperature) to an entropic barrier (at high temperature).

The positions of the $T\,S$ values for the activated state in Fig. 6c are uncertain, because they depend on the pre-exponential factor in the Eyring equation, which is $k_B T/h = 6\times10^{12}$ s^{-1} at 25 °C. Based on the rates of contact formations in proteins, Bieri and Kiefhaber suggest that the maximal rate of protein folding (and thus the pre-exponential factor in the Eyring equation) might be near 10^8 s^{-1} [11]. We therefore calculated the $T\,S$ values also with this factor. As expected, the entropic barrier becomes smaller by approximately 25 kJ/mol (Fig. 6d), but the fundamental result that refolding is limited by an enthalpy barrier at low temperature and by an entropy barrier at high temperature remains unaffected, even though the pre-exponential factor in the Eyring equation was changed by more than four orders of magnitude.

We used the viscosity data for urea solutions (Fig. 4 and Table 1) to correct our previously measured [25] kinetic data for the unfolding and refolding of *Bs*-CspB (Table 2). The reaction profiles based on the viscosity-corrected data for $\Delta C_p^{\ddagger}$, $\Delta H^{\ddagger}$ and $\Delta S^{\ddagger}$ are shown in Fig. 8 in comparison to the values for *Bc*-Csp. By the ΔC_p criterion, the activated state is approximately 85% native-like for *Bs*-CspB, but only 63% native-like for *Bc*-Csp. The $\Delta C_p^{\ddagger}$ values are, however, derived from the second derivative of the temperature dependence of the measured rate constants and therefore must be interpreted with due care.

The data for the activation enthalpies and entropies (Table 2 and Fig. 8b,c) give a very clear answer. Although *Bc*-Csp is approximately twice as stable (at 25 °C) as its mesophilic counterpart *Bs*-CspB, still the refolding reactions of the two proteins show almost identical rates, activation enthalpies and activation entropies, and the activated states of refolding are both approximately 90% native by the *m* value criterion. This suggests

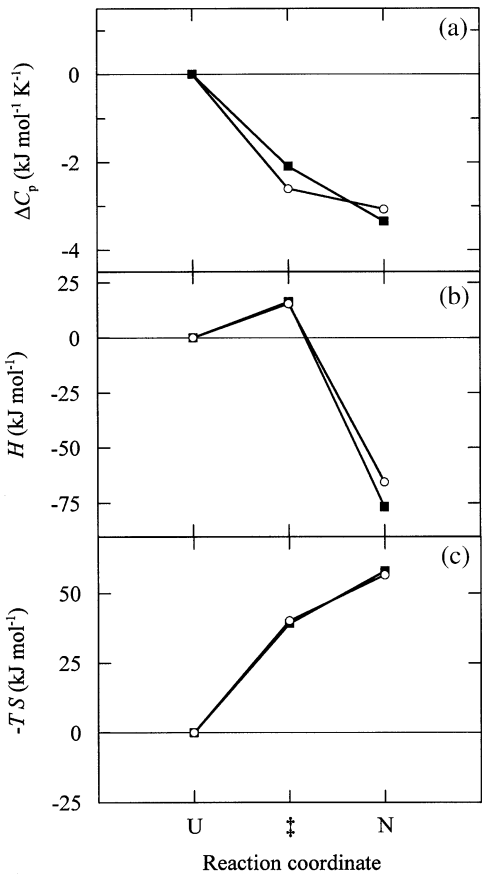

Fig. 8. Reaction profiles for the folding reaction of *Bc*-Csp (■) and *Bs*-CspB (○) in 0 M GdmCl, pH 7.0, as obtained after the viscosity correction of the apparent rate constants. The parameters were calculated from the difference relative to the values for the unfolded state U as in Fig. 6. The heat capacity [panel (a)] was assumed to the independent of temperature. The enthalpy H [panel (b)] and the entropic term $-T\,S$ [panel (c)] are shown for 25 °C. The data for *Bs*-CspB were taken from Schindler and Schmid [25], and corrected for solvent viscosity.

that the two proteins show almost identical activated states of folding. In unfolding, *Bc*-Csp resembles *Bs*-CspB in the activation entropy, but the activation enthalpy is increased by 12 kJ/mol (25 °C). This suggests a very simple explanation for the difference in stability (approx. 10 kJ/mol, Table 2) between *Bs*-CspB and *Bc*-Csp. It originates from additional enthalpic interactions at the protein surface that are established in native *Bc*-Csp only after the molecules passed through the activated state. Remember that all sequence differences between the two proteins are at the surface.

The energy barrier in protein folding is caused by a slight asynchrony between the entropy and enthalpy. Chain entropy is lost early when the protein folds into an approximately native conformation, but the enthalpy is harvested only when all the native interactions are established at the end of the folding process. Our comparison has identified several surface residues that contribute to this final gain in enthalpic interactions.

4. Conclusions

Diffusional protein folding reactions should be analyzed on the basis of Kramers' theory rather than by TST, which was developed for reactions of small molecules in the gas phase. Analyses based on TST are, however, very popular because this theory links kinetics with equilibrium thermodynamics, and provides numbers for the free energies, enthalpies and entropies of activation. Analyses by Kramers' theory and by TST are not mutually exclusive. After the appropriate corrections, TST can still be used to calculate numbers for the activation parameters of diffusional protein folding reactions.

The Gibbs free energies of activation, $\Delta G^{\ddagger}$, are hardly affected by these comparisons when the relative viscosity of water at 25 °C is set as one. The $m^{\ddagger}$ value (the dependence of $\Delta G^{\ddagger}$ on denaturant concentration) of unfolding is slightly increased after the viscosity correction, but the resulting change in the α-value ($\alpha = m^{\ddagger}_{UN}/(m^{\ddagger}_{UN} - m^{\ddagger}_{NU})$ is much smaller than 0.10.

The values for $\Delta H^{\ddagger}$ and $T\Delta S^{\ddagger}$ are affected more strongly, but in a predictable fashion by the temperature dependence of solvent viscosity, and the respective corrections are easily derived from pseudo-Arrhenius analyses of viscosity data as in Fig. 4b. It indicates that the measured values for $\Delta H^{\ddagger}$ must be decreased by 17.1 kJ/mol, and those for $T\Delta S^{\ddagger}$ increased by the same amount (at 25 °C, where the relative viscosity of the solvent is 1). Neglect of the viscosity effect leads to an overes-

timate of the enthalpic and an underestimate of the entropic barrier to folding. In the presence of a denaturant, solvent viscosity increases less strongly with temperature, and the correction for $\Delta H^{\ddagger}$ drops slightly from approximately 17 to 14 kJ/mol, when the GdmCl concentration is increased from 0 to 7 M. This drop primarily affects unfolding kinetics that are measured at high denaturant concentration.

The viscosity effects can be accounted for either before the analysis by correcting the apparent rate constants, or afterwards by subtracting the pseudothermodynamic parameters from the Eyring analysis of the viscosity data (Table 1) from the calculated activation parameters.

The numbers for $\Delta H^{\ddagger}$ are virtually independent of the kinetic theory used. For unimolecular reactions they are determined directly by the temperature dependence of the measured rate constants. The values for $T\Delta S^{\ddagger}$ depend on the pre-exponential factors in the various rate laws, and in TST a reduction of the pre-exponential factor by four orders of magnitude decreases $T\Delta S^{\ddagger}$ by 23 kJ/mol (Fig. 6d). It is reassuring to see that even such a large change does not affect the fundamental conclusion that the refolding barrier of the cold shock proteins changes from being enthalpic at low temperature (2 °C) to being entropic at high temperature (50 °C).

Such a change in the nature of the folding barrier has been proposed in theoretical models of folding [39,40]. These models focus on the changes within the folding protein chain itself and often neglect the changes in the solvent. These changes are, however, responsible for the decrease in heat capacity during folding and thus determine the decrease of enthalpy and entropy of folding with temperature [41]. In an analogous manner, the decreases with temperature of the activation enthalpy and activation entropy of refolding, reflect the differences in the solvation of the unfolded and the activated state of folding. Not chain folding itself, but the changes in the solvent that accompany formation of the activated state lead to the change from an enthalpic to an entropic barrier. It is thus a consequence of the hydrophobic effect.

Makhatadze and Privalov [42,43] decomposed the overall stability of folded proteins into individual contributions. Based on their numbers we estimate a loss in chain entropy upon folding of *Bc*-Csp equivalent to approximately $-T\Delta S = 1\times10^3$ kJ/mol. Compared with this estimate, the experimental $T\Delta S^{\ddagger}$ values in the range of -50 to $+50$ kJ/mol are extremely small, revealing that the loss in chain entropy during folding is compensated by a large increase in solvent entropy, which for *Bc*-Csp is estimated as $T\Delta S = 500$ kJ/mol. These crude calculations indicate that the activated state of folding resembles the native state, in the sense that large individual contributions to enthalpy and entropy largely compensate each other. Thus, the shift from a 70 kJ/mol enthalpic barrier at 2 °C to a 70 kJ/mol entropic barrier at 50 °C, is caused by a slight asynchrony of the energy balance.

Acknowledgments

This work was supported by grants from the Slovak Grant Agency VEGA (grant no. 7023), from the Deutsche Forschungsgemeinschaft, and the Fonds der Chemischen Industrie. We thank the members of our groups for fruitful discussions.

References

[1] V. Daggett, A.J. Li, L.S. Itzhaki, D.E. Otzen, A.R. Fersht, Structure of the transition state for folding of a protein derived from experiment and simulation, J. Mol. Biol. 257 (1996) 430–440.

[2] V.P. Grantcharova, D.S. Riddle, J.V. Santiago, D. Baker, Important role of hydrogen bonds in the structurally polarized transition state for folding of the src SH3 domain, Nat. Struct. Biol. 5 (1998) 714–720.

[3] D.S. Riddle, V.P. Grantcharova, J.V. Santiago, E. Alm, I. Ruczinski, D. Baker, Experiment and theory highlight role of native state topology in SH3 folding, Nat. Struct. Biol. 6 (1999) 1016–1024.

[4] D.E. Kim, Q. Yi, S.T. Gladwin, J.M. Goldberg, D. Baker, The single helix in protein L is largely disrupted at the rate-limiting step in folding, J. Mol. Biol. 284 (1998) 807–815.

[5] R.E. Burton, G.S. Huang, M.A. Daugherty, T.L. Calderone, T.G. Oas, The energy landscape of a fast-folding protein mapped by Ala–Gly substitutions, Nat. Struct. Biol. 4 (1997) 305–310.

[6] J.C. Martinez, L. Serrano, The folding transition state between SH3 domains is conformationally restricted and evolutionarily conserved, Nat. Struct. Biol. 6 (1999) 1010–1016.
[7] V. Villegas, J.C. Martinez, F.X. Aviles, L. Serrano, Structure of the transition state in the folding process of human procarboxypeptidase A2 activation domain, J. Mol. Biol. 283 (1998) 1027–1036.
[8] M.E. Milla, B.M. Brown, C.D. Waldburger, R.T. Sauer, P22 arc repressor: transition state properties inferred from mutational effects on the rates of protein unfolding and refolding, Biochemistry 34 (1995) 13914–13919.
[9] C. Tanford, Part B. The transition state from native to denatured state, Adv. Protein Chem. 23 (1968) 218–282.
[10] C.R. Matthews, Pathways of protein folding, Ann. Rev. Biochem. 62 (1993) 653–683.
[11] O. Bieri, T. Kiefhaber, Kinetic models in protein folding, in: R.H. Pain (Ed.), Mechanisms of Protein Folding, Oxford University Press, Oxford, 2000, pp. 34–64.
[12] W. Teschner, R. Rudolph, J.-R. Garel, Intermediates on the folding pathway of octopine dehydrogenase from *Pecten jacobaeus*, Biochemistry 26 (1987) 2791–2796.
[13] H. Vaucheret, L. Signon, G. Lebras, J.-R. Garel, Mechanism of renaturation of a large protein, aspartokinase–homoserine dehydrogenase, Biochemistry 26 (1987) 2785–2790.
[14] B.A. Chrunyk, C.R. Matthews, Role of diffusion in the folding of the alpha subunit of tryptophan synthase from *Escherichia coli*, Biochemistry 29 (1990) 2149–2154.
[15] M. Jacob, T. Schindler, J. Balbach, F.X. Schmid, Diffusion control in an elementary protein folding reaction, Proc. Natl. Acad. Sci. USA 94 (1997) 5622–5627.
[16] M. Jacob, M. Geeves, G. Holtermann, F.X. Schmid, Diffusional barrier crossing in a two-state protein folding reaction, Nat. Struct. Biol. 6 (1999) 923–926.
[17] R.P. Bhattacharyya, T.R. Sosnick, Viscosity dependence of the folding kinetics of a dimeric and monomeric coiled coil, Biochemistry 38 (1999) 2601–2609.
[18] K.W. Plaxco, D. Baker, Limited internal friction in the rate-limiting step of a two-state protein folding reaction, Proc. Natl. Acad. Sci. USA 95 (1998) 13591–13596.
[19] H.A. Kramers, Brownian motion in a field of force and the diffusion model of chemical reactions, Physica 7 (1940) 284–304.
[20] M. Jacob, F.X. Schmid, Protein folding as a diffusional process, Biochemistry 38 (1999) 13773–13779.
[21] M. Karplus, D.L. Weaver, Diffusion–collision model for protein folding, Biopolymers 18 (1979) 1421–1437.
[22] D.K. Klimov, D. Thirumalai, Viscosity dependence of the folding rates of proteins, Phys. Rev. Lett. 79 (1997) 317–320.
[23] H. Schindelin, M.A. Marahiel, U. Heinemann, Universal nucleic acid-binding domain revealed by crystal structure of the *B. subtilis* major cold-shock protein, Nature 364 (1993) 164–168.
[24] T. Schindler, M. Herrler, M.A. Marahiel, F.X. Schmid, Extremely rapid folding in the absence of intermediates: the cold-shock protein from *Bacillus subtilis*, Nat. Struct. Biol. 2 (1995) 663–673.
[25] T. Schindler, F.X. Schmid, Thermodynamic properties of an extremely rapid protein folding reaction, Biochemistry 35 (1996) 16833–16842.
[26] D. Perl, U. Mueller, U. Heinemann, F.X. Schmid, Two exposed amino acid residues confer thermostability on a cold shock protein, Nat. Struct. Biol. 7 (2000) 380–383.
[27] U. Mueller, D. Perl, F.X. Schmid, U. Heinemann, Thermal stability and atomic-resolution crystal structure of the *Bacillus caldolyticus* cold shock protein, J. Mol. Biol. 297 (2000) 975–988.
[28] D. Perl, C. Welker, T. Schindler, et al., Conservation of rapid two-state folding in mesophilic, thermophilic, and hyperthermophilic cold shock proteins, Nat. Struct. Biol. 5 (1998) 229–235.
[29] H. Schindelin, M. Herrler, G. Willimsky, M.A. Marahiel, U. Heinemann, Overproduction, crystallization, and preliminary X-ray diffraction studies of the major cold shock protein from *Bacillus subtilis*, CspB, Proteins Struct. Funct. Genet. 14 (1992) 120–124.
[30] L.M. Mayr, O. Landt, U. Hahn, F.X. Schmid, Stability and folding kinetics of ribonuclease T1 are strongly altered by the replacement of *cis*-proline 39 with alanine, J. Mol. Biol. 231 (1993) 897–912.
[31] M.M. Santoro, D.W. Bolen, Unfolding free energy changes determined by the linear extrapolation method. 1. Unfolding of phenylmethanesulfonyl α-chymotrypsin using different denaturants, Biochemistry 27 (1988) 8063–8068.
[32] R.C. Weast, Handbook of Chemistry and Physics, 55 ed, CRC Press, Cleveland, OH, USA, 1974.
[33] C.N. Pace, D.V. Laurents, A new method for determining the heat capacity change for protein folding, Biochemistry 28 (1989) 2520–2525.
[34] K. Kawahara, C. Tanford, Viscosity and density of aqueous solutions of urea and guanidine hydrochloride, J. Biol. Chem. 241 (1966) 3228–3232.
[35] J.K. Myers, C.N. Pace, J.M. Scholtz, Denaturant m values and heat capacity changes: relation to changes in accessible surface areas of protein unfolding, Protein Sci. 4 (1995) 2138–2148.
[36] H.R. Bosshard, E. Durr, T. Hitz, I. Jelesarov, Energetics of coiled coil folding: the nature of the transition states, Biochemistry 40 (2001) 3544–3552.
[37] G.I. Makhatadze, P.L. Privalov, Protein interactions with urea and guanidinium chloride — a calorimetric study, J. Mol. Biol. 226 (1992) 491–505.
[38] G.I. Makhatadze, P.L. Privalov, Energetics of protein structure, Adv. Protein Chem. 47 (1995) 307–425.
[39] J.D. Bryngelson, J.N. Onuchic, N.D. Socci, P.G. Wolynes, Funnels, pathways, and the energy landscape of

protein folding: a synthesis, Proteins Struct. Funct. Genet. 21 (1995) 167–195.
[40] M. Karplus, A. Sali, Theoretical studies of protein folding and unfolding, Curr. Opin. Struct. Biol. 5 (1995) 58–73.
[41] P.L. Privalov, Stability of proteins, Adv. Protein Chem. 33 (1979) 167–241.
[42] G.I. Makhatadze, P.L. Privalov, Hydration effects in protein unfolding, Biophys. Chem. 51 (1994) 291–309.
[43] G.I. Makhatadze, P.L. Privalov, On the entropy of protein folding, Protein Sci. 5 (1996) 507–510.
[44] P.J. Kraulis, MOLSCRIPT: a program to produce both detailed and schematic plots of protein structures, J. Appl. Crystallogr. 24 (1991) 946–950.